NJC

Accepted Manuscript

This is an *Accepted Manuscript*, which has been through the Royal Society of Chemistry peer review process and has been accepted for publication.

Accepted Manuscripts are published online shortly after acceptance, before technical editing, formatting and proof reading. Using this free service, authors can make their results available to the community, in citable form, before we publish the edited article. We will replace this *Accepted Manuscript* with the edited and formatted *Advance Article* as soon as it is available.

You can find more information about *Accepted Manuscripts* in the Information for Authors.

Please note that technical editing may introduce minor changes to the text and/or graphics, which may alter content. The journal's standard Terms & Conditions and the Ethical guidelines still apply. In no event shall the Royal Society of Chemistry be held responsible for any errors or omissions in this *Accepted Manuscript* or any consequences arising from the use of any information it contains.

ROYAL SOCIETY OF CHEMISTRY

www.rsc.org/njc

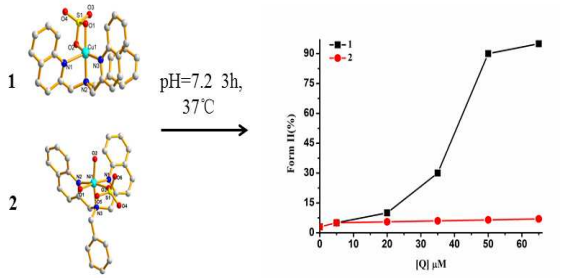

Difference of redox active metal result in some discrepancy for their complexes in biological activity.

Significant differences in biological activity of mononuclear Cu(II) and Ni(II) complex with polyquinolinyl ligand

Jun-Ling Li[a, b, d], Lin Jiang[a, b, c], Bi-Wei Wang[a, b, c], Jin-Lei Tian[a, b, c, d*], Wen Gu[a, b], Xin Liu[a, b, c*] and Shi-Ping Yan[a,b]

[a] *Department of Chemistry, Nankai University, Tianjin 300071, People's Republic of China*

[b] *Tianjin Key Laboratory of Metal and Molecule Based Material Chemistry, Tianjin 300071, People's Republic of China*

[c] *Key Laboratory of Advanced Energy Materials Chemistry (MOE), Tianjin 300071, People's Republic of China*

[d] *Collaborative Innovation Center of Chemical Science and Engineering (Tianjin)*

Abstract

Two new mononuclear complexes [Cu**L**(η^2-SO_4)] (**1**) and [Ni**L**(η-SO_4)(H_2O)$_2$]·H_2O·CH_3CH_2OH (**2**), where **L** is bis(2-quinolinyl methyl) benzyl-amine, have been synthesized and characterized by X-ray crystallography, ESI-MS and elemental analysis techniques. Complex **1** possesses a distorted square pyramidal geometry while complex **2** possesses distorted octahedral geometry. Interestingly, **2** only dissolves in DMF-H_2O mixed solvent, while **1** shows good water solubility. Both electronic absorption and EB displacement assay show that complexes could bind with CT-DNA through partial intercalation. Though DNA-binding abilities of **1** and **2** are similar, their chemical nuclease activities exhibit a great difference. Under physiological conditions, **1** could effectively convert pBR322 plasmid DNA from Form I to Form II at about 50 μM without any external agent, which shows self-oxidation cleavage activity; however, **2** shows poor DNA cleavage activity at 75 μM even in the presence of H_2O_2. At the same time, **1** also displays about 11-fold more potent than **2** against HeLa cells with IC_{50} value **1** (6.89 μM) and **2 (**74.85 μM). The IC_{50} value of **1** is even lower than the widely used drug cisplatin. The redox activity of Cu(II) and Ni(II) may play the main role in the biological

activity of two complexes, but the exact mechanism is still unclear. In addition, interactions of complexes with BSA have also been explored by fluorescence and UV-visible spectroscopic methods. The results indicated that complexes could quench the intrinsic fluorescence of BSA in a static quenching process.

Introduction

In 2008, about 7.6 million deaths (around 13% of all deaths) have been caused by cancer, while the number is projected to rise above 13.1 million in 2030.[1] As a result, considerable attempts have been made to explore metal-based complexes for cancer therapy.[2-4] Among them, many transition metal complexes attract great attentions owing to their possible applications as new cancer therapeutic agents.[5-8] Copper and Nickel, as a bioessential transitional metal, their respective complexes have been investigated on the assumption that endogenous metals may be less toxic for normal cells with respect to cancer cells. Recently, Carlo Santini[9] and his coworkers have elaborated on the advances of copper-based complexes as anticancer drugs. L. N. Ji[10] have reported several Cu(II) complexes by introduction of aryl-modified 2,6-di(thiazol-2-yl) pyridine, notably all the complexes show excellent cytotoxic activities on the BEL-7402 and HepG2 cells. Moreover, one mononuclear Cu(II) complex $[Cu(ttpy)(Gly)(NO_3)]\cdot(NO_3)\cdot H_2O$ (ttpy=4'-p-tolyl-2,2':6,2''-terpyridine) shows remarkable cleavage activity in the presence of Vc, which has been reported by Z. J. Guo.[11] At the same time, many nickel complexes have also been investigated for their good DNA binding and cleavage activity.[12, 6, 13] However, compared with Ni(II), Cu(II) is a redox active metal ion, which is much more easy to reduce Cu(II) to Cu(I) than to reduce or oxidize Ni(II). As a result, some differences in biological abilities usually exist between Cu(II) and Ni(II) complexes. For example, with same ligand, mononuclear Cu(II)-bpy (2,2'-bipyridine) complex exhibits more active ability in cleaving BNPP at pH = 7 and pH = 8.6 than Ni(II)-bpy complex,[14] while Ni(II) complex displays better DNA binding ability than Cu(II) complex by incorporation ligand N,N'-bis-5-(triethylammonium methyl)-salicy-lidene-2,3-naphthalendiiminato).[6] It will be interesting to investigate interactions between DNA and Cu(II), Ni(II) complexes with same ligand.

The square-pyramidal Cu(II) complex with the neutral, non-deprotonated chelating ligand bis(2-pyridylmethyl) amine (dpa) have been investigated for their effective DNA scissor and

anticancer agents.[15] The derivative of dpa, N-benzyl di(pyridylmethyl) amine (phdpa) was used to synthesize several Cu(II) complexes, which also show good anticancer properties and could cause the fragmentation of nucleus.[16] Complexes with the family of dpa, with which substituents may be introduced on the imino nitrogen atom, have been investigated by many groups for their effective breakage of DNA duplex.[17-19] Compared with pyridine, the quinoline ring shows better planarity and stronger hydrophobic DNA interaction, which may show better DNA binding ability. Moreover, the quinoline skeleton, isolated from Camptotheca acuminate, shows important biological activities.[20, 21] Therefore, substitution pyridine with quinoline in the dpa may provide a new insight for developing new metallodrugs. However, so far few literatures have reported potential anticancer activity of complexes with quinoline derivatives of dpa.

On the other hand, protein forms the basis of material in virtually all living organisms. In addition, serum albumin plays an important role in drug delivery, with capacity to reversibly bind a large variety of drugs results in its prevailing role in drug pharmacokinetics and pharmacodynamics.[22] BSA, bovine serum albumin, has been investigated extensively for its structural homology with human serum albumin (HSA).[23, 24] Therefore, it is greatly valuable to explore the interaction between BSA and compounds.

All the above facts have stimulated our interest in the present work on synthesizing two mononuclear complexes [Cu**L**(η^2-SO_4)] (**1**) and [Ni**L**(η-SO_4)$(H_2O)_2$]·H_2O·CH_3CH_2OH (**2**), with **L** (bis(2-quinolinyl methyl) benzyl-amine). Though several complexes[25, 26] have been synthesized with **L**, few attempts have been made to explore the biological properties. In this work, we have investigated and explored some biological activities of two complexes. Notably, two complexes display several significant differences: (i) **1** shows better water solubility than **2**; (ii) **1** exhibits good self-oxidation DNA cleavage ability, while **2** shows poor DNA cleavage activity even in the presence of activators; (iii) **1** also displays about 11-fold more potent than **2** against HeLa cells. Furthermore, the affinity of complex to BSA was also investigated via various spectroscopic methods (fluorescence quenching and UV-visible). The great difference between two complexes, especially in the DNA cleavage activity, may be due to the redox activity of center metals, Cu(II) is more effective in the formation of ROS species than Ni(II). We hope all the results may contribute to further studies for how compounds act in biological systems.

Experimental

Materials and measurements

All reagents and chemicals were purchased from commercial sources and used as received. Agarose, pBR322 plasmid DNA, ethidium bromide (EB), bovine serum albumin (BSA) and calf thymus CT-DNA were obtained from Sigma. Stock solutions of **1** (1.0×10^{-3} M in H_2O) and **2** (1.0×10^{-3} M in 20%DMF-H_2O mixed solvent) were stored at 4 °C and prepared to required concentrations for all experiments. Ultra-pure MilliQ water (18.24 MΩ·cm) was used in all experiments. Tris-HCl and phosphate buffer solution were prepared using ultrapure water. Elemental analysis for C, H and N were obtained on a Perkin-Elmer analyzer model 240. Infrared spectroscopy on KBr pellets were performed on a Bruker Vector 22 FT-IR spectrophotometer in the 4000-400 cm^{-1} regions. Thermogravimetric analysis was performed on NETZSCH TG 209 in the region 25-800 °C with 10 K/min. Electrospray ionization mass spectrometry (ESI-MS) was obtained on Agilent 6520 Q-TOF LC/MS. Electronic spectra were measured on a JASCO V-570 spectrophotometer. Fluorescence spectral data were obtained on a MPF-4 fluorescence spectrophotometer at room temperature. The Gel Imaging and documentation DigiDoc-It System were assessed using Labworks Imaging and Analysis Software (UVI, UK).

Insert Scheme 1(Schematic structures of phdpn(left) and **L**(right).)

Synthesis of ligand L and corresponding complexes

Preparation of ligand

The **L** (Scheme 1) was prepared according to a procedure described in the literature[26] with some improvements.A mixture of 2-chloromethylquinoline hydrochloride (1.82 g, 8.4 mmol), benzylamine (0.45 g, 4.2 mmol) and potassium carbonate (3.50 g, 26. 0mmol) in acetonitrile (30 mL) was refluxed for 48 hours. After solvent was removed under reduced pressure, the residue was separated by chloroform/water and organic phase was dried, evaporated, and pale yellow powder was obtained. Selected IR data (KBr, ν, cm^{-1}): 1638(s), 1617(s), 1117(m), 824(m), 620(s).

Synthesis of [CuL(η^2-SO_4)] (1)

To an ethanol solution (10 ml) of **L** (0.04 g, 0.1 mmol), an aqueous solution (5 mL) of $CuSO_4 \cdot 5H_2O$ (0.03 g, 0.1 mmol) was added. The resulting mixture was stirred for 3 h at room temperature. Blue prism crystals suitable for X-ray diffraction were obtained by slow evaporation of filtrate after seven days, which were collected by filtration, washed with diethyl ether and dried in air, yield 0.02 g (38%). Elemental analysis (%): calc. for $C_{27}H_{23}N_3O_4SCu$: C, 59.06; H, 4.22; N, 7.65. Found: C, 58.08; H, 4.32; N, 7.34. Selected IR data (KBr, ν, cm^{-1}): 1638(s), 1618(s), 1222(m), 1136(s), 826(m), 623(s). ESI-MS (m/z=497.11, [Cu**L**(CH_3CH_2OH)-H]$^+$).

Synthesis of [NiL(η-SO_4) $(H_2O)_2$]·3(H_2O)·CH_3CH_2OH (2)

Complex **2** was prepared by a procedure similar to that given in the case of **1**, using $NiSO_4 \cdot 6H_2O$ (0.03 g, 0.1 mmol) in place of $CuSO_4 \cdot 5H_2O$ to the reaction mixture. Cyan block crystals suitable for X-ray diffraction were obtained by slow evaporation of filtrate after ten days, which were collected by filtration, washed with diethyl ether and dried in air, yield 0.03 g (43%). Elemental analysis (%): calc. for $C_{29}H_{39}N_3O_{10}SNi$: C, 51.19; H, 5.78; N, 6.18. Found: C, 50.28, H, 5.64; N, 6.35. Selected IR data (KBr, ν, cm^{-1}): 1638(s), 1618(s), 1179(m), 621(s). ESI-MS (m/z=492.12, [Ni**L**(CH_3CH_2OH)-H]$^+$).

X-ray crystallographic studies

Single-crystal X-ray diffraction data of compounds were collected on a Bruker Smart 1000 CCD diffractometer using Mo-K_α radiation (λ = 0.71073 Å) with the ω scan technique. The structures were solved by direct methods (SHELXS-97 and refined with full-matrix least-squares technique on F^2 using the SHELXL-97.[27, 28] The hydrogen atoms were added theoretically, and riding on the concerned atoms and refined with fixed thermal factors. For **2**, the *PLANTON SQUEEZE* procedure[29] was applied to treat the highly distorted solvent H_2O molecules in the crystal structure. The application of SQUEEZE gave a good improvement in the data statistics and allowed for a full anisotropic refinement of both structure models. TG analysis has been carried out to prove the possible water molecules in the outside. The result suggests that three water molecules and one ethanol molecule exist (Fig.S1). The details of crystallographic data and structure refinement parameters are summarized in Table 1, and selected bond angles and distances are listed in Table 2. Crystallographic data for complexes have been deposited with the

Cambridge Crystallographic Data Centre with the corresponding CCDC reference number for **1**-**2**: 1028398-1028399.

DNA binding and cleavage activity studies

The UV absorbance at 260 nm and 280 nm of the CT-DNA solution in (5 mM Tris, 50 mM NaCl pH = 7.2) gives a ratio of 1.8~1.9, indicating that CT-DNA was sufficiently free of protein.[30] The concentration of CT-DNA was determined from its absorption intensity at 260 nm with a molar extinction coefficient of 6600 $M^{-1}cm^{-1}$. The absorption spectra of complex binding to DNA were performed by increasing amounts of CT-DNA to complex in Tris-HCl buffer.

The relative binding abilities of complex to CT-DNA were studied with an EB-bound CT-DNA system in (5 mM Tris, 50 mM NaCl pH = 7.2). The experiment was carried out by titrating certain volume of a stock complex into EB-DNA solution containing 2.4×10^{-6} M EB and 48×10^{-6} M CT-DNA. Then fluorescence spectra were recorded at room temperature with excitation at 510 nm and emission at about 602 nm after the system was allowed to equilibrate for 5 min.

DNA cleavage experiment was carried out by agarose gel electrophoresis and performed by incubation at 37°C as follows: pBR322 DNA (0.1 μg/μL) in 50 mM Tris-HCl /18 mM NaCl buffer (pH = 7.2) was treated with complex **1**-**2**. Different concentrations of complex were added to DNA stock. Then samples were incubated for 3 h, and loading buffer was added. Last, samples were electrophoresed for 2 h at 0.9% agarose gel using Tris-boric acid-EDTA buffer. After electrophoresis, bands were visualized by UV light and photo-graphed.

Cleavage mechanism investigation of pBR322 DNA was investigated in the presence of some radical scavengers and reaction inhibitors. The reactions were conducted by adding standard radical scavengers of KI, NaN_3, SOD, EDTA and groove binding agent Methyl Green (for major groove), SYBR Green (for minor groove) to pBR322 DNA after the addition of complex. Cleavage experiment was initiated by addition of complex and quenched with 2 μL of loading buffer. Further analysis was carried out by the above standard method.

Protein Binding Studies

Fluorescence quenching experiments have been carried out to investigated interaction between BSA and complex **1**-**2**, by using bovine serum albumin stock solution (BSA, 1.5 mM) in 10 mM phosphate buffer (pH = 7.0). The fluorescence spectra were recorded at room temperature

with excitation wavelength of BSA at 280 nm and the emission at 342 nm by keeping concentration of BSA constant (29.4 μM) while varying complex concentration from 0 to 40 μM for **1**-**2**.

In Vitro Cell Assay

The cytotoxicity assay of **1** and **2** against cervical carcinoma cells (HeLa) was evaluated by a CCK-8 kit assay. HeLa cells were cultured in a DMEM/F12 medium supplemented with 10% fetal bovine serum (5% CO_2 at 37 °C). Cells were seeded into 96-well plates at a density of 10^4cell/well and incubated for 48 h to allow cell attachment. Then, cells were washed with PBS, and medium was replaced with a fresh medium containing the indicated concentrations of either **1** or **2**. Cells without pretreatment were used as the control. After a period of incubation, cells were washed with PBS and incubated in DMEM/F12 with 10% WST-8 solution for another 2 h. The absorbance of each well was measured at a wavelength of 450 nm with a plate reader. The results were expressed as the mean values of three measurements. The cell viability was calculated as follows

$$\text{cell viability}(\%) = \frac{I_{sample} - I_{blank}}{I_{control} - I_{blank}} \times 100$$

where I_{sample} , I_{control} , and I_{blank} represent the absorbance intensity at 450 nm determined for cells treated with different samples, for control cells (nontreated), and for blank wells without cells (the same amounts of CCK-8 solution and sample solution as the sample wells were added to the blank wells), respectively.

Results and discussion

Two new mononuclear complexes **1** and **2** have been synthesized by using one reported ligand **L**. The crystals for complexes suitable for X-ray analysis were collected after about one week. The polyquinolinyl based complexes shows good DNA binding ability due to large planar ligands, Cu(II) complex even demonstrates good self-activation DNA cleavage activity and anticancer activity.

Description of the crystal structure

Complex has been structurally characterized by X-ray crystallography (Fig. 1), the details of data collection conditions and parameters of refinement process are given in Table 1, and selected bond lengths and angles are given in Table 2, respectively.

Insert Fig. 1 (Molecular structures of complexes; (a) for complex **1**, (b) for complex **2**; Hydrogen atoms, solvent molecules have been omitted for clarity.),

Table 1(Crystal data and structure refinement for complex **1** and **2**.)

and Table 2 (Selected bond lengths [Å] and angles [°] for complex **1** and **2**.)

Complex **1** and **2** are mononuclear compounds but show different crystal structures. Complex **1** crystallized in monoclinic cell with *C*2/*c* space group. The Cu^{2+} center shows pentacoordinated geometry with a N_3O_2 donor unit derived from one tertiary amine N, two quinoline N atoms and two O atoms from SO_4^{2-}. The τ value of Cu is 0.04, which display a slightly distorted square pyramidal geometry. The base square position were occupied by O(1) and O(2) from SO_4^{2-}(Cu(1)-O(1) 1.976(3) Å, Cu(1)-O(2) 2.008(3) Å), N(2) and N(3) from **L** (Cu(1)-N(2) 2.017(4) Å, Cu(1)-N(3) 2.040(3) Å). The bond distances fall in the ranges of several reported Cu(II) complexes.[31, 32] The N(1) atom from another quinoline ring of **L** (Cu(1)-N(1) 2.251(4) Å) occupies the apical site. The axial Cu(1)-N(1) bond distance is longer than the equatorial Cu(1)-N(3) bond, which may be due to d_{x2-y2} orbital in a Cu^{2+} square pyramidal geometry contains two electrons while d_{z2} orbital only one electron.[32]

The Ni^{2+} center exhibits hexacoordinated geometry in complex **2**, which is different from **1**. The N_3O_3 donor set is constituted by one tertiary amine N, two quinolyl-N atoms and one O atom from SO_4^{2-}, two O atoms from two distinct H_2O molecules, which shows a distorted octahedral environment. The basal plane is formed by N(1)N(3)O(1)O(2) (Ni(1)-N(1) 2.104(3) Å, Ni(1)-N(3) 2.116(3) Å, Ni(1)-O(1) 2.064(3) Å, Ni(1)-O(2) 2.065(3) Å), the apical position are occupied by the O(3) (Ni(1)-O(3) 2.110(3) Å) and N(2)(Ni(1)-N(2) 2.122(3) Å). The bond distances fall in the range of several Ni^{2+} complexes.[33] The bond distance Ni(1)-O(1), Ni(1)-O(2) is almost the same, which is shorter than Ni(1)-O(3) (2.110(3) Å)， which may be the smaller steric hindrance for H_2O molecule than SO_4^{2-}. Hydrogen bonds were formed by the coordinated H_2O, SO_4^{2-} and solvent ethanol molecule. The geometrical parameters for hydrogen bonds are reported in Table 3.

Related bond distances and θ angles of O–H…O type all fall in the range of some reported complexes.[34] The hydrogen bonds are all O–H…O type with θ angles considerably shorter than 180°.

Insert Fig. 2 (Depiction of the Hydrogen bonds interactions in **2**.) and Table 3(Hydrogen bonds [Å and °] of complex **2**.)

DNA-binding and cleavage activities

DNA-binding studies

Electronic absorption studies

Electronic absorption spectroscopy was an effective method in examining binding mode of DNA with metal complex. The potential binding ability of complex **1**-**2** with CT-DNA was characterized by measuring their effects on UV absorption. The typical titration curve for complex **1**-**2** is shown in Fig. 3. It is clear that **1** has two strong absorptions at *ca*. 204 nm and 233 nm, and a weak absorption at *ca*. 305 nm. However, DMF in solution of complex **2** shows strong influence at *ca*. 200-250 nm because of strong absorption. So here we investigated the absorption at *ca*. 305 nm for complex **2**. The insets in Fig. 3 are the typical titration curves and plots of $(\varepsilon_a - \varepsilon_f)/(\varepsilon_b - \varepsilon_f)$ versus [DNA] for titration of CT-DNA to complex. Upon incremental addition of CT-DNA to **1**-**2**, a decrease in molar absorptivity (hypochromism, 20.7 % and 11.1 %) for two complexes appeared. Such marked change in the intensity of spectral bands is expected an intimate association of complex with CT-DNA. In order to determine the binding strength of complexes with CT-DNA, intrinsic binding constants K_b were calculated from a nonlinear fitting according to the equation.[35]

$$(\varepsilon_a - \varepsilon_f)/(\varepsilon_b - \varepsilon_f) = \left(b - \left(b^2 - 2K_b{}^2 C_t[DNA]/s\right)^{1/2}\right)/2K_b C_t \qquad (1a)$$

$$b = 1 + K_b C_t + K_b[DNA]/2s \qquad (1b)$$

The DNA binding constant (K_b) values of complexes, along with the binding site sizes (s), are given in Table 4. The K_b values of complexes are similar **1** (3.56×10^5 M^{-1}) and **2** (3.19×10^5 M^{-1}), which may be due to their similar structures in solution. From Table 4, the K_b values of our compounds are stronger than $[Cu(L^6)Cl_2]$ (L^6=2-(1H-benzimidazol-2-yl)ethyl-(4,4a-dihydroquinolin-2-ylmethy-lene)amine), which may be due to the hydrophobic interaction of

phenyl and the quinolyl moiety [32] in our ligand. The DNA affinity of **2** is also stronger compared to several mononuclear Ni(II) complexes.[36, 12] The binding site size (*s*) values obtained from the fit, which shows a measure of the number of DNA bases associated with complex. The low *s* values ($s<1$) was attributed to the aggregation of hydrophobic molecule on DNA surface.[37] According to the electronic absorption studies, it has been found that complexes maybe bind to DNA by partial intercalation; however, some more experiments should be carried out for further proving the binding mode.

Insert Fig. 3 (Absorption spectra of complexes in the absence (dashed line) and presence (solid line) of increasing amounts of CT-DNA (9.4-65.8 μM for **1**, 9.4-75.2 μM for **2**) in 5 mM Tris-HCl/50 mM NaCl buffer (pH = 7.2). A for **1**(15 μM) and B for **2**(50 μM)), the arrow shows the absorbance changes on increasing DNA concentration. The insert shows the least-squares fit of $(\varepsilon_a-\varepsilon_f)/(\varepsilon_b-\varepsilon_f)$ vs [DNA] for complex.)

and Table 4 (Absorption spectral properties and Fluorescence spectral properties of complex **1**-**2** bound to CT-DNA.)

Fluorescence spectral studies

The DNA binding behavior of complex **1** and **2** was further investigated by fluorescence spectral titration method. EB-DNA system generally appears a significant increase in the fluorescence emission when EB bounds to DNA, and a decrease appears when EB is displaced by another DNA intercalate molecule.[38, 39] From Fig. 4 and Fig. S2, as the titration of complex **1** and **2**, a dramatic hypochromism effect appeared at 603 nm, which suggests EB may be replaced from the system and the binding may involves some intercalative interaction. Quenching data is in agreement with the classical linear Stern–Volmer equation,[40] $I_0 / I = 1+ K_{sv}[Q]$, where I_0 and I represent the fluorescence intensities in the absence and presence of quencher and $[Q]$ is the quencher concentration. In the linear fit plot of I_0 / I versus $[Q]$, K_{sv} is the Stern–Volmer dynamic quenching constant. The apparent DNA binding constant (K_{app}), which could express the degree of affinity toward DNA, was calculated on the basis of equation.

$$K_{EB}[EB] = K_{app}[complex]$$

Here $K_{EB} = 1.0 \times 10^7\ M^{-1}$, ([EB] = 2.4 μM). K_{EB} is the binding constant of EB to DNA, and [complex] is the value concentration of complex at 50% reduction of fluorescence intensity for EB.

The K_{sv} and K_{app} values for complex **1** and **2** were listed in Table 4. Approximate K_{app} values of **1**(1.23×10^6 M^{-1}) and **2**(1.21×10^6 M^{-1}) verify further the rationality of K_b values in UV-visible method. Upon replacement pyridyl moiety in [(phdpa)Cu(bpy)(ClO_4)] (3.69×10^4 M^{-1}) and [(phdpa)Cu(phen)(H_2O)] (8.20×10^4 M^{-1})[16] by quinolyl in **1** and **2**, the DNA binding affinities of complex increase significantly, which is supported by the stronger hydrophobic DNA interaction and larger aromaticity of quinolyl than pyridyl moiety.

Insert Fig. 4 (Emission spectra of EB bound to CT-DNA in the absence (dashed line) and presence (solid lines) of complex **1** (0-70 μM) in (5 mM Tris, 50 mM NaCl pH = 7.2) buffer. Inset: the plot of I_0 / I versus the complex concentration.)

DNA Cleavage Activity

Cleavage of pBR322 DNA by complexes

The DNA cleavage experiment of complex **1** and **2** was investigated using supercoiled pBR322 plasmid DNA by electrophoresis in a medium of 50 mM Tris–HCl/18 mM NaCl buffer (pH=7.2). Fig. 5(a) shows the electrophoresis results of DNA cleavage induced by increasing concentrations of **1** without addition of any external redox agent. When the concentration is lower than 20 μM, DNA cleavage ability is poor, but when it is above 35 μM, DNA breakage activity of **1** increase significantly. Complex **1** almost completely converts supercoiled form (Form I) to its open circular form (Form II) at 50 μM concentration. However, under same conditions (Fig. 5(b)), complex **2** shows almost no effect on the cleavage of DNA even at 65 μM. In order to investigate whether the external redox agent could affect efficient DNA cleavage activity for **2**, activator H_2O_2 was added to the reaction. However, in the presence of H_2O_2, complex **2** still shows lower activity than **1**, only converting about 50% Form I to Form II at the highest concentration assayed (75 μM) (Fig. S2). The results demonstrate that both complexes show DNA cleavage activity, but complex **1** shows higher activity than **2**(Fig. 5(c)), which suggests that the metal ions may play an important role in the DNA cleavage. For two metal ions in our complex, Cu(II) is more effective in reduction Cu(II) to Cu(II) than to reduce or oxidize Ni(II), which may result in the difference in DNA cleavage activity.

Insert Fig. 5 (Cleavage of plasmid pBR322 DNA (0.1 μg/μL) at different concentrations of complex after 3h incubation at 37 °C ((a) for **1**, (b) for **2**); Line 0: DNA control, Line 1-5: DNA+ complex (5, 20, 35, 50, 65 μM); (c) the percentage of Form II versus concentrations of **1**(■) and **2**(●).)

DNA Cleavage Mechanism

The activity of DNA-cleaving complexes without an oxidant or reducing agent is often related to a hydrolytic rather than oxidative mechanism. However, without a co-regent, there are still many complexes that act by an oxidative mechanism.[41-45] As a result, the possible ROS responsible for the DNA cleavage were investigated using common agent like KI, DMSO as hydroxyl radical scavengers; L-Histidine, NaN_3 as a singlet oxygen ($^1O_2$) quencher; superoxide dismutase (SOD) as $O_2^{\cdot -}$ radical scavenger. The experiment was also carried out in the presence of a major groove binder agent, methyl green; a minor groove binder, SYBR green; and the metal ion chelating agent, EDTA.

From Fig. 6, the cleavage activity of complex **1** and **2** is reduced dramatically in the presence of KI and EDTA, indicating that ˙OH radicals and the metal ions may play the key role in the cleavage process. For complex **1**, addition of L-His also prevents the cleavage, indicating that singlet oxygen is also involved in the cleavage mechanism.[11] Methyl green efficiently inhibits the process, which implies that complex **1** may bind to DNA in major groove. However, for **2**, the binding position may be in minor groove. In conclusion, ˙OH radicals are the crucial ROS responsible for the cleavage activity of two complexes; singlet oxygen is less influential in the cleavage for **1**; metal ions also act as an important role in the process; however, the exact mechanism is still unknown.

Insert Fig. 6 (Bar diagram shows the cleavage of DNA by complex **1** (50 μM), and **2** (50 μM + 0.25 mM H_2O_2) in the presence of different inhibitors.)

Protein binding activities

Fluorescence quenching of BSA by complex

Investigation on the binding of a drug with protein will facilitate interpretation of the metabolism and transporting process of a drug and to explain the relationship between structures and functions of a protein. Bovine serum albumin (BSA) was utilized extensively as a result of its structural homology with human serum albumin (HSA). Qualitative analysis of the binding of chemical compounds to BSA is usually detected by inspecting the fluorescence spectra. The interaction of complex **1** and **2** with BSA has been studied from the concentration dependence of the change in the fluorescence intensity of protein upon the addition of complexes. Fluorescence spectra were recorded in the range of 290-450 nm upon excitation at 280 nm. The effect of the fluorescence intensity of BSA by the complex **1** is shown in Fig. 7. (Fig. S6 for **2**)

Upon addition of **1**-**2** to the solution of BSA, a significant decrease of fluorescence intensity has been observed. Fluorescence intensity of BSA at 350 nm was decreased about 55.3% (complex **1**) and 54.8% (complex **2**) from the initial fluorescence intensity of BSA, which suggested a definite interaction of compounds with BSA protein.[46] To study the quenching process, fluorescence quenching data were analyzed with Stern-Volmer equation. The quenching constant K_{sv} could be calculated by the Stern-Volmer equation: $I_0/I = 1+K_{sv}[Q]$, where I_0 and I are the fluorescence intensities of fluorophore in the absence and presence of quencher, respectively, K_{sv} is observed by using the plot of I_0 / I versus [Q] (Fig. 8). Moreover, based on the Scachard equation:

$$\log [(I_0-I)/I] = \log K + n\log [Q]$$

Where K is the binding constant of compound with DNA and n is the number of binding sites. The number of binding sites (n) and binding constant (K) have been obtained from the plot of log $(I_0-I) / I$ versus log[Q]. The calculated K_{sv}, K, n values are given in Table 5. The value of n is around 1, which indicated existence of just one single binding site in BSA for the complex.[47] The K values of complexes is smaller than several reported mononuclear complexes.[48, 47]

Insert Fig. 7 (Fluorescence emission spectra of the BSA (29.4 μM) system in the absence (dashed line) and presence (solid lines) of complex **1** (0-40 μM).),

Fig. 8 (The plot of I_0 / I versus the concentration of complex **1-2**; **(b)** Plot of log$(I_0 - I) / I$ vs. log [Q] for BSA in the presence of complex **1-2**. (**1**(■), **2**(●)))

and Table 5 (The quenching constants, binding constants and number of binding sites for the interaction of complex **1**-**2** with BSA.)

UV-vis absorption spectroscopy

UV-vis visible absorption spectroscopy is a simple method to explore quenching mechanism of BSA by the interaction with complexes. If the fluorophore and quencher come into contact during the transient existence of the exited state, the dynamic quenching happens; however, if the fluorophore-quencher complex was formed in the ground state, it will be the static quenching. Electronic spectra of BSA with complexes are shown in Fig. S7. After addition of complexes, a slight enhancement in the absorption intensity was observed, which suggests static quenching process may happen between complex and BSA.[24]

In Vitro Cell Cytotoxicity

The in vitro cytotoxicity against HeLa cells of complex **1** and **2** was carried out by CCK-8 assay. The CCK-8 assay is a well-established method for determination of cell viability in cell proliferation and cytotoxicity assays,[49, 50] which utilizes Dojindo's highly water-soluble tetrazolium salt, WST-8, to produce water-soluble fornazan dye on reduction in the living cells to determine the number of cells. The results have been analyzed by means of cell inhibition expressed as IC_{50} values. After incubation for 48 h, **1**(6.89 μM) shows about 11-fold lower IC_{50} value than **2**(78.4 μM). Notably, **1** even exhibits remarkably high cytotoxicity against HeLa cell than cisplain with about 2 times lower IC_{50} value than cisplain(15 μM)[51], which indicates that **1** look like a potential metal-based anticancer drug. However, further studies are still needed to assess the actual mechanism of biological activity of **1**.

Conclusion

Two new mononuclear complexes have been synthesized and characterized in this work. Crystal structure of **2** is different with **1** as a result of coordination of water molecules; but they show similar structure in solution, moreover, complex **1** show good water solubility than **2**. Two complexes show similar DNA binding abilities, which has been investigated by absorption and fluorescence measurements. However, a great difference appeared in their DNA cleavage

activities. Complex **1** could make DNA cleaved effectively without the activator, while with the same concentration, complex **2** makes only about 50% fragmentation of DNA in the presence of external agents such as H_2O_2. We conclude difference in redox activity of metal ions may play an important role in cleavage process. So cleavage mechanism assays have been carried out by introduction of ROS inhibitors. The results suggest that hydroxyl radical was proposed as the main ROS involved in the cleavage mechanism and metal ions also play an important role in the process. However, exact DNA cleavage mechanism is unknown, further investigations are still needed. According to the results obtained from fluorescence and UV-vis spectrometry, we speculate that complexes could bind with BSA in a static quenching process. Notably, **1** shows a considerable cytotoxic activity (IC_{50}=6.89 μM) against HeLa cells even better than cisplatin, which suggests that **1** may be one potential anticancer drug. The difference in electronic configuration for Cu ($d^{10}s^1$) and Ni (d^8s^2) resulted in their different redox activity: it is much more easy to reduce Cu(II) to Cu(I) than to reduce or oxidize Ni(II) and Cu(II) is an excellent Fenton catalyst while Ni(II) is very poor. Incorporation of redox active and inactive metal in compounds may result difference in the biological activity, we hope the result may contribute to further investigations of how compounds work in biological system.

Acknowledgments

This work was supported by the National Natural Science Foundation of China (21171101, 21371103 and 21471085), Tianjin Science Foundation (No. 12JCYBJC13600), NFFTBS (No. J1103306) and MOE Innovation Team (IRT13022) of China.

References

1 World Health Organization, Cancer, *WHO Press: Geneva, 2013*, Fact sheet No. 297.

2 K. D. Mjos and C. Orvig, *Chem. Rev.*, 2014, **114**, 4540.

3 M. F. Primik, S. Göschl, S. M. Meier, N. Eberherr, M. A. Jakupec, A. Enyedy, G. Novitchi and V. B. Arion, *Inorg. Chem.*, 2013, **52**, 10137.

4 M. A. Sgambellone, A. David, R. N. Garner and K. R. Dunbar, C. Turro, *J. Am. Chem. Soc.*, 2013, **135**, 11274.

5 U. Basu, I. Khan, A. Hussain, B. Gole, P. Kondaiah and A. R. Chakravarty, *Inorg. Chem.*, 2014, **53**, 2152.

6 A. Lauria, R. Bonsignore, A. Terenzi, A. Spinello, F. Giannici, A. Longo, A. M. Almerico and G. Barone, *Dalton Trans.*, 2014, **43**, 6108.

7 I. E. Leon, A. L. Di Virgilio, V. Porro, C. I. Muglia, L. G. Naso, P. M. Williams, M. Bollati-Fogolin and S. B. Etcheverry, *Dalton Trans.*, 2013, **42**, 11868.

8 M. L. Zastrow and V. L. Pecoraro, *Biochemistry*, 2014, **53**, 957.

9 C. Santini, M. Pellei, V. Gandin, M. Porchia, F. Tisato and C. Marzano, *Chem. Rev.*, 2014, **114**, 815.

10 L. Li, K. Du, Y. Wang, H. Jia, X. Hou, H. Chao and L. N. Ji, *Dalton Trans.*, 2013, **42**, 11576.

11 W. Zhou, X. Wang, M. Hu and Z. J. Guo, *J. Inorg. Biochem.*, 2013, **121**, 114.

12 M. Kyropoulou, C. P. Raptopoulou, V. Psycharis and G. Psomas, *Polyhedron*, 2013, **61**, 126.

13 J. Tan, L. Zhu and B. Wang, *Dalton Trans.*, 2009, 4722.

14 M. D. Rosch and A. W. C. Trogler, *Inorg. Chem.*, 1990, **29**, 2409.

15 M. M. Ibrahim, A. M. M. Ramadan, G. M. Mersal and S. A. El-Shazly, *J. Mol. Struct.*, 2011, **998**, 1.

16 Q. Y. Chen, H. J. Fu, W. H. Zhu, Y. Qi, Z. P. Ma, K. D. Zhao and J. Gao, *Dalton Trans.*, 2011, **40**, 4414.

17 C. Y. Gao, X. Qiao, Z. Y. Ma, Z. G. Wang, J. Lu, J. L. Tian, J. Y. Xu and S. P. Yan, *Dalton Trans.*, 2012, **41**, 12220.

18 Q. Jiang, N. Xiao, P. Shi, Y. Zhu and Z. J. Guo, *Coord. Chem. Rev.*, 2007, **251**, 1951.

19 Y. Zhao, J. Zhu, W. He, Z. Yang, Y. Zhu, Y. Li, J. Zhang and Z. J. Guo, *Chem. Eur. J.*, 2006, **12**, 6621.

20 M. Ozyanik, S. Demirel, H. Bektas, N. Demirbas and S. A. Karaoglu, *Turki. J. Chem.*, 2012, **36**, 233.

21 G. P. Volynets, M. O. Chekanov, A. R. Synyugin, A. G. Golub, O. P. Kukharenko, V. G. Bdzhola and S. M. Yarmoluk, *J. Med. Chem.*, 2011, **54**, 2680.

22 O. K. Abou-Zied and O. I. K. Al-Shihi, *J. Am. Chem. Soc.*, 2008, **130**, 10793.

23 A. Patra, T. K. Sen, A. Ghorai, G. T. Musie, S. K. Mandal, U. Ghosh and M. Bera, *Inorg. Chem.*, 2013, **52**, 2880.

24 S. M. T. Shaikh, J. Seetharamappa, S. Ashoka and P. B. Kandagal, *Dyes and Pigments*, 2007, **73**, 211.

25 A. S. Kunishita, T. Osako, Y. Tachi, J. Teraoka and A. S. Itoh, *Bull. Chem. Soc. Jpn.*, 2006, **79**, 1729.

26 S. V. Kryatov, S. Taktak, I. V. Korendovych and E. V. Rybak-Akimova, *Inorg. Chem.*, 2005, **44**, 85.

27 G. M. Sheldrick, *University of Göttingen, Germany*, 1997.

28 G. M. Sheldrick, *University of Göttingen, Germany*, 1997.

29 A. L. Spek, *J. Appl. Crystallogr.*, 2003, **36**, 7.

30 J. Marmur, *J. Mol. Biol.*, 1961, **2**, 1961.

31 R. Kannappan, S. Tanase, I. Mutikainen, U. Turpeinen and J. Reedijk, *Inorg. Chim. Acta*, 2005, **358**, 383.

32 C. Rajarajeswari, R. Loganathan, M. Palaniandavar, E. Suresh, A. Riyasdeen and M. A. Akbarsha, *Dalton Trans.*, 2013, **42**, 8347.

33 J. Adhikary, P. Chakraborty, S. Das, T. Chattopadhyay, A. Bauzá, S. K. Chattopadhyay, B. Ghosh, F. A. Mautner, A. Frontera and D. Das, *Inorg. Chem.*, 2013, **52**, 13442.

34 M. Kyropoulou, C. P. Raptopoulou, V. Psycharis and G. Psomas, *Polyhedron*, 2013, **61**, 126.

35 M. T. Carter, M. Rodriguez and A. J. Bard, *J. Am. Chem. Soc.*, 1989, **111**, 8901.

36 G. J. Chen, Z. G. Wang, Y. Y. Kou, J. L. Tian and S. P. Yan, *J. Inorg. Biochem.*, 2013, **122**, 49.

37 A. M. Angeles-Boza, P. M. Bradley, K. L. Fu, S. E. Wicke, J. Bacsa, K. R. Dunbar and C. Turro, *Inorg. Chem.*, 2004, **43**, 8510.

38 F. J. Meyer-Almes and D. Porschke, *Biochemistry*, 1993, **32**, 4246.

39 R. F. Pasternack, M. Caccam, B. Keogh, T. A. Stephenson, A. P. Williams and A. E. J. Gibbst, *J. Am. Chem. Soc.*, 1991, **113**, 6835.

40 J. R. Lakowicz and A. G. Weber, *Biochemistry.*, 1973, **12**, 4161.

41 P. U. Maheswari, K. Lappalainen, M. Sfregola, S. Barends, P. Gamez, U. Turpeinen, I. Mutikainen, G. P. Van Wezel and J. Reedijk, *Dalton Trans.*, 2007, 3676.

42 P. U. Maheswari, S. Roy, H. D. Dulk, S. Barends, G. V. Wezel, B. Kozlevc, P. Gamez and J. Reedijk, *J. Am. Chem. Soc.*, 2006, **128**, 710.

43 P. P. Silva, W. Guerra, J. N. Silveira, A. M. D. C. Ferreira, T. Bortolotto, F. L. Fischer, H. N. Terenzi, A. Neves and E. C. Pereira-Maia, *Inorg. Chem.*, 2011, **50**, 6414.

44 S. Borah, M. S. Melvin, N. Lindquist and A. R. A. Manderville, *J. Am .Chem. Soc.*, 1998, **120**, 4557.

45 J. Tan, B. Wang and L. Zhu, *J. Biol. Inorg. Chem.*, 2009, **14**, 727.

46 R. D. Senthil, G. Paramaguru, N. S. P. Bhuvanesh, J. H. Reibenspies, R. Renganathan and K. Natarajan, *Dalton Trans.*, 2011, **40**, 4548.

47 R. D. Senthil, N. S. P. Bhuvanesh and K. Natarajan, *Inorg. Chem.*, 2011, **50**, 12852.

48 M. Alagesan, N. S. P. Bhuvanesh and N. Dharmaraj, *Dalton Trans.*, 2013, **42**, 7210.

49 M. Liong, J. Lu, M. Kovochich, T. Xia, S. G. Ruehm, A. E. Nel, F. Tamanoi and J. I. Zink, *ACS Nano*., 2008, **2**, 889.

50 L. Yuan, W. Chen, J. Hu, J. Z. Zhang and D. Yang, *Langmuir*, 2013, **29**, 734.

51 R. W. Y. Sun, A. L. F. Chow, X. H. Li, J. J. Yan, S. S. Y. Chui and C. M. Che, *Chem. Sci.*, 2011, **2**, 728.

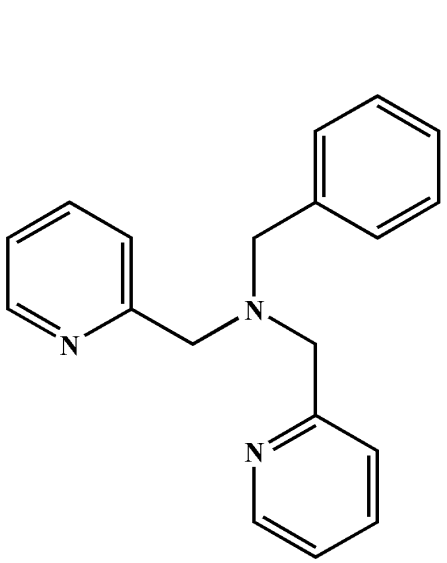

phdpn

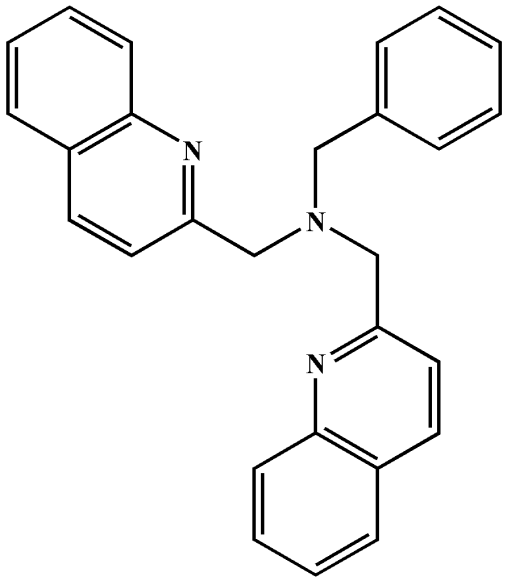

L

Scheme 1 Schematic structures of phdpn(left) and **L**(right).

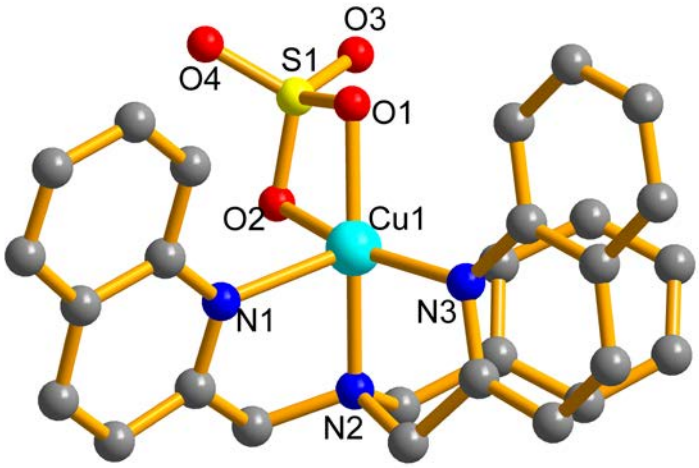

(a)

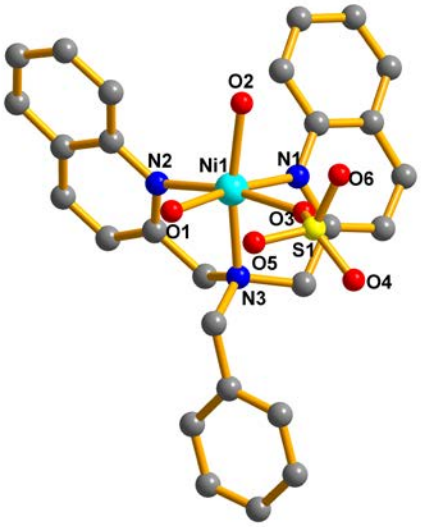

(b)

Fig. 1 Molecular structures of complexes; (a) for complex **1**, (b) for complex **2**. Hydrogen atoms, solvent molecules have been omitted for clarity.

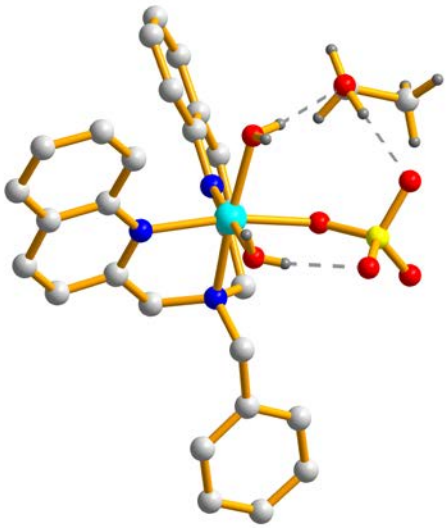

Fig. 2 Depiction of the Hydrogen bonds interactions in **2**.

Table 1 Crystal data and structure refinement for complex **1** and **2**.

Compound reference	**1**	**2**
Chemical formula	$C_{27}H_{23}CuN_3O_4S$	$C_{29}H_{33}N_3NiO_{10}S$
Formula Mass	549.08	679.17
T/K	293(2)	113(2)
Crystal system	Monoclinic	Monoclinic
Space group	*C2/c*	*P2(1)/n*
a/Å	26.919(5)	14.772(3)
b/Å	8.7230(17)	13.805(3)
c/Å	22.424(5)	14.786(3)
α/°	90.00	90.00
β/°	107.99(3)	96.14(3)
γ/°	90.00	90.00
V/Å^3	5008.2(17)	2992.4(11)
No. of formula units per unit cell, *Z*	8	4
D/*g/cm*^{3}	1.456	1.390
μ/mm^{-1}	0.994	0.768
No. of reflections measured	16212	29820
No. of independent reflections	4419	5253
R_{int}	0.0919	0.0728
Final R_1 values ($I > 2\sigma(I)$)	0.0567	0.0448
Final $wR(F^2)$ values ($I > 2\sigma(I)$)	0.1150	0.1036
Final R_1 values (all data)	0.0869	0.0496
Final $wR(F^2)$ values (all data)	0.1274	0.1066

Table 2 Selected bond lengths [Å] and angles [°] for complex **1** and **2**.

1		**2**	
Cu(1)-O(1)	1.976(3)	Ni(1)-O(1)	2.064(3)
Cu(1)-O(2)	2.008(3)	Ni(1)-O(2)	2.065(3)
Cu(1)-N(2)	2.017(4)	Ni(1)-N(1)	2.104(3)
Cu(1)-N(3)	2.040(3)	Ni(1)-O(3)	2.110(3)
Cu(1)-N(1)	2.251(4)	Ni(1)-N(3)	2.116(3)
O(1)-Cu(1)-O(2)	71.49(11)	Ni(1)-N(2)	2.122(3)
O(1)-Cu(1)-N(2)	165.09(12)	O(1)-Ni(1)-O(2)	90.91(11)
O(2)-Cu(1)-N(2)	95.87(13)	O(1)-Ni(1)-N(1)	173.31(12)
O(1)-Cu(1)-N(3)	104.17(13)	O(2)-Ni(1)-N(1)	93.83(12)
O(2)-Cu(1)-N(3)	162.58(13)	O(1)-Ni(1)-O(3)	89.64(12)
N(2)-Cu(1)-N(3)	85.52(14)	O(2)-Ni(1)-O(3)	85.17(12)
O(1)-Cu(1)-N(1)	108.79(13)	N(1)-Ni(1)-O(3)	86.07(11)
O(2)-Cu(1)-N(1)	93.70(12)	O(1)-Ni(1)-N(3)	96.47(12)
N(2)-Cu(1)-N(1)	79.20(14)	O(2)-Ni(1)-N(3)	169.74(12)
N(3)-Cu(1)-N(1)	103.60(13)	N(1)-Ni(1)-N(3)	78.25(12)
		O(3)-Ni(1)-N(3)	87.76(12)
		O(1)-Ni(1)-N(2)	88.17(13)
		O(2)-Ni(1)-N(2)	105.39(13)
		N(1)-Ni(1)-N(2)	95.10(12)
		O(3)-Ni(1)-N(2)	169.24(12)
		N(3)-Ni(1)-N(2)	82.03(12)

Table 3 Hydrogen bonds [Å and °] of complex **2**.

D-H…A	d(D–H)	d(H…A)	d(D…A)	θ(< DHA)
O1-H1B…O5	0.717	1.973	2.669	163.89
O2-H2B…O7	0.817	1.954	2.762	170.14
O7-H7A…O6	0.820	1.944	2.762	174.63

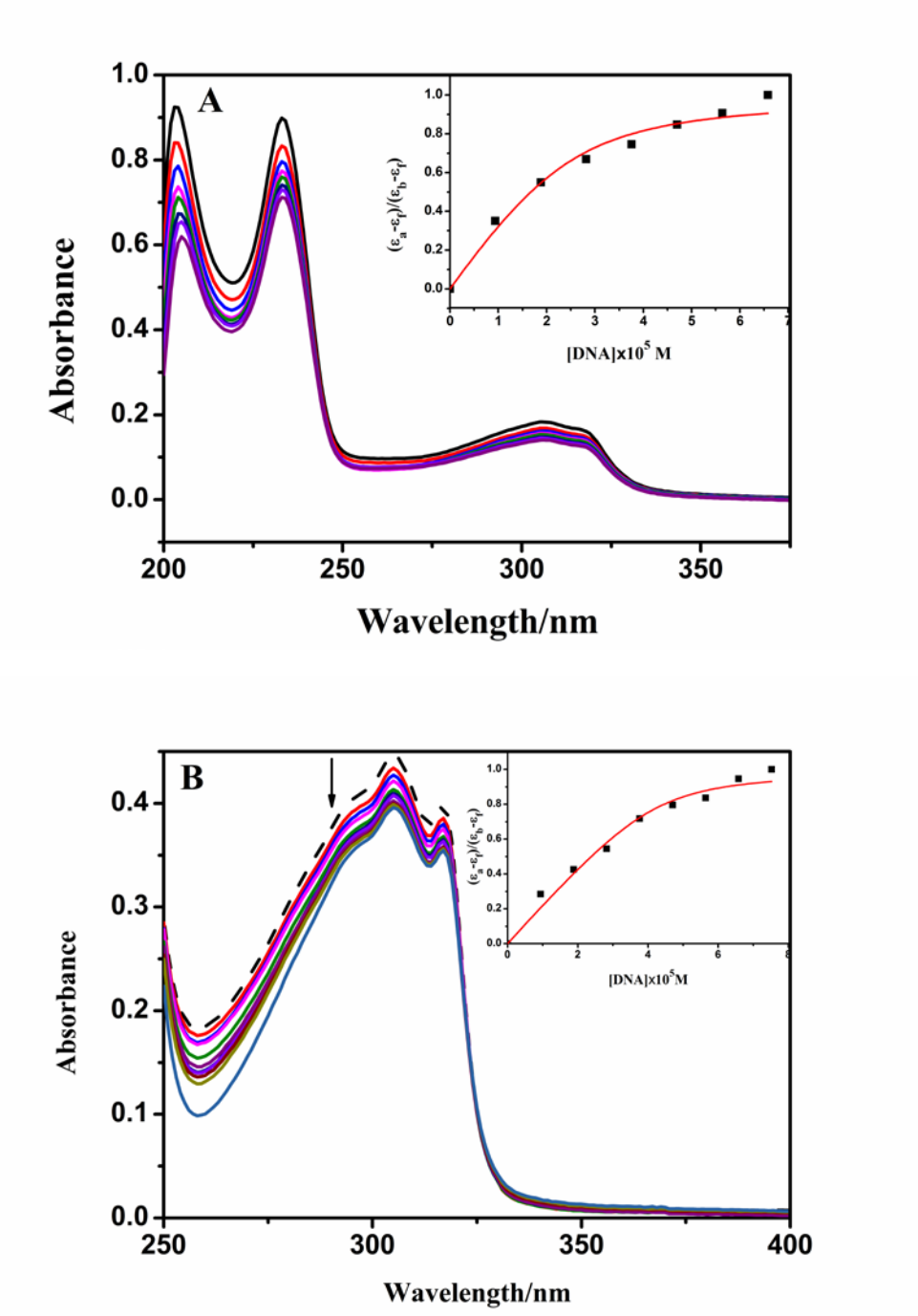

Fig. 3 Absorption spectra of complexes in the absence (dashed line) and presence (solid line) of increasing amounts of CT-DNA (9.4-65.8 μM for **1**, 9.4-75.2 μM for **2**) in 5 mM Tris-HCl/50 mM NaCl buffer (pH = 7.2). A for **1**(15 μM) and B for **2**(50 μM)), the arrow shows the absorbance changes on increasing DNA concentration. The insert shows the least-squares fit of $(\varepsilon_a-\varepsilon_f)/(\varepsilon_b-\varepsilon_f)$ vs [DNA] for complex.

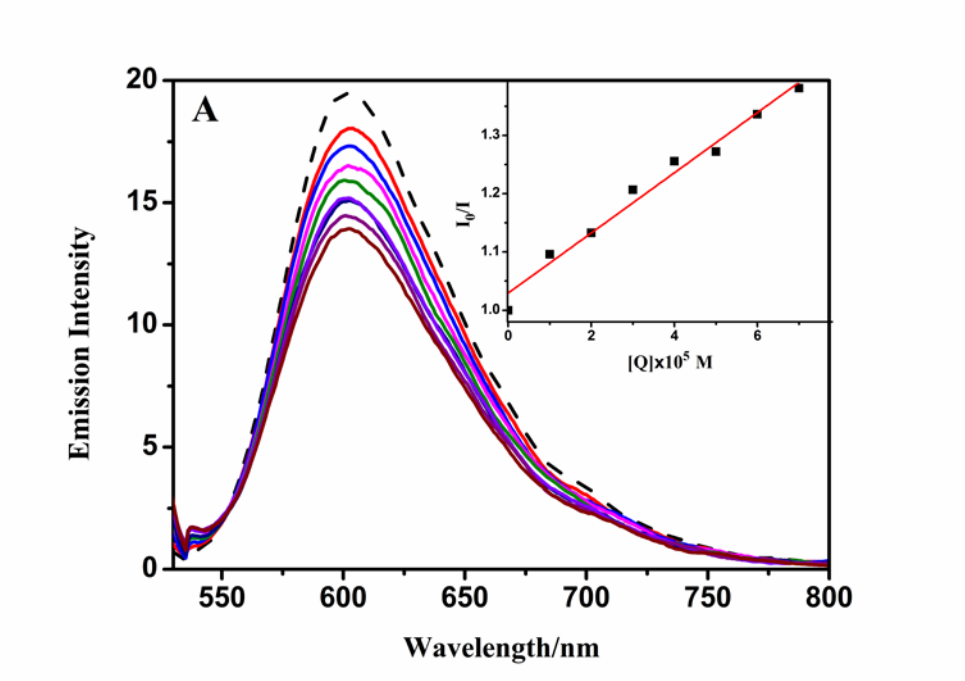

Fig. 4 Emission spectra of EB bound to CT-DNA in the absence (dashed line) and presence (solid lines) of complex **1** (0-70 μM) in (5 mM Tris, 50 mM NaCl pH = 7.2) buffer. Inset: the plot of I_0 / I versus the complex concentration.

Table 4 Absorption spectral properties and Fluorescence spectral properties of complex **1-2** bound to CT-DNA.

complex	$K_b(M^{-1})$	$K_{app}(M^{-1})$	Ref
1	3.56×10^5	1.23×10^6	this work
2	3.19×10^5	1.21×10^6	this work
[(phdpa)Cu(bpy)(ClO_4)]		3.69×10^4	16
[(phdpa)Cu(phen)(H_2O)]		8.20×10^4	16
[Cu(L^3)Cl_2]		3.40×10^4	32
[Cu(L^6)Cl_2]	6.60×10^3	7.60×10^4	32
[Ni(dicl)$_2$(bipy)]	2.21×10^5		12
[Ni(Phterpy)$_2$]	7.64×10^3	1.43×10^5	36

Phdpa: N -benzyl di(pyridylmethyl)amine

L^3: (2-pyridin-2-yl-ethyl)pyridin-2-ylmethyleneamine

L^6: 2-(1H -benzimidazol-2-yl)ethyl-(4,4a-dihydroquinolin-2-ylmethy-lene)amine

Dicl: sodium diclofenac

Phterpy: 4'-phenyl-2,2':6',2''-terpyridine

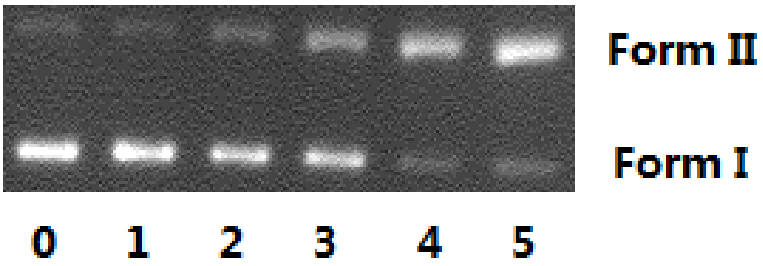

(**a**)

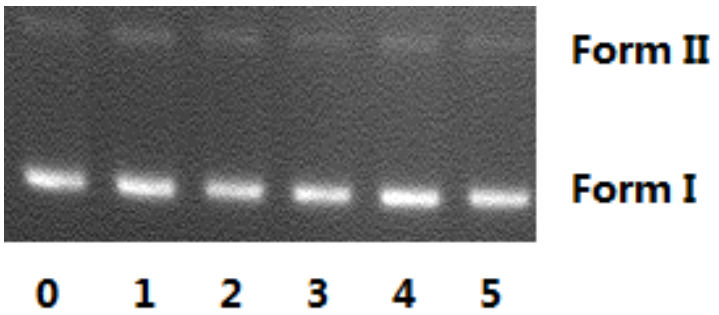

(**b**)

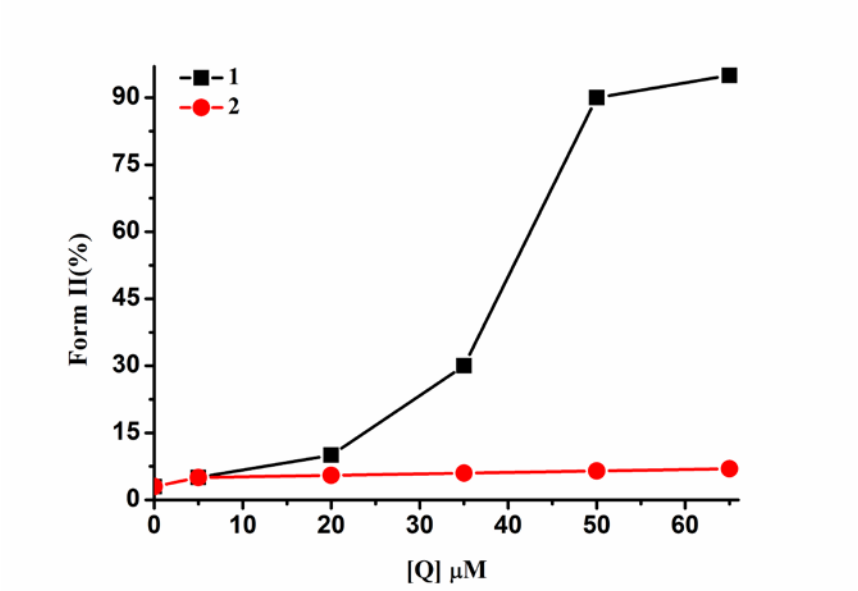

(**c**)

Fig. 5 Cleavage of plasmid pBR322 DNA (0.1 μg/μL) at different concentrations of complex after 3h incubation at 37 °C ((a) for **1**, (b) for **2**); Line 0: DNA control, Line 1-5: DNA+ complex (5, 20, 35, 50, 65 μM); (c) the percentage of Form II versus concentrations of **1** (■) and **2** (●).

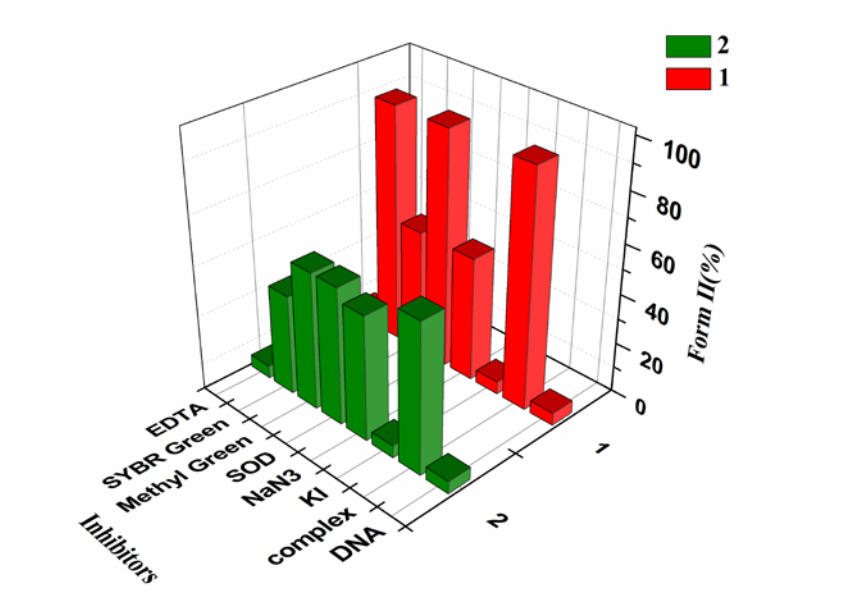

Fig. 6 Bar diagram shows the cleavage of DNA by complex **1** (50 μM), and **2** (50 μM + 0.25 mM H_2O_2) in the presence of different inhibitors.

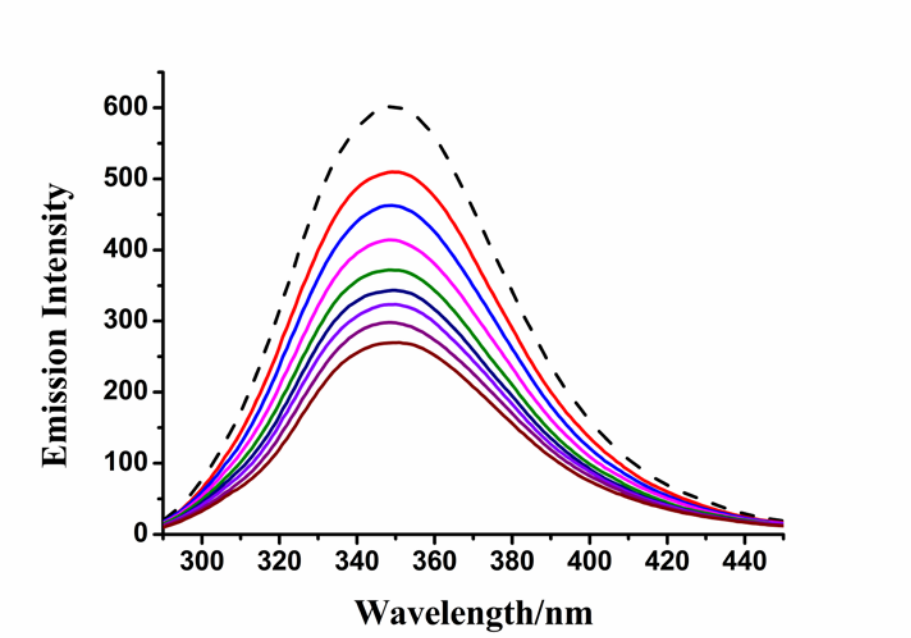

Fig. 7 Fluorescence emission spectra of the BSA (29.4 μM) system in the absence (dashed line) and presence (solid lines) of complex **1** (0-40 μM).

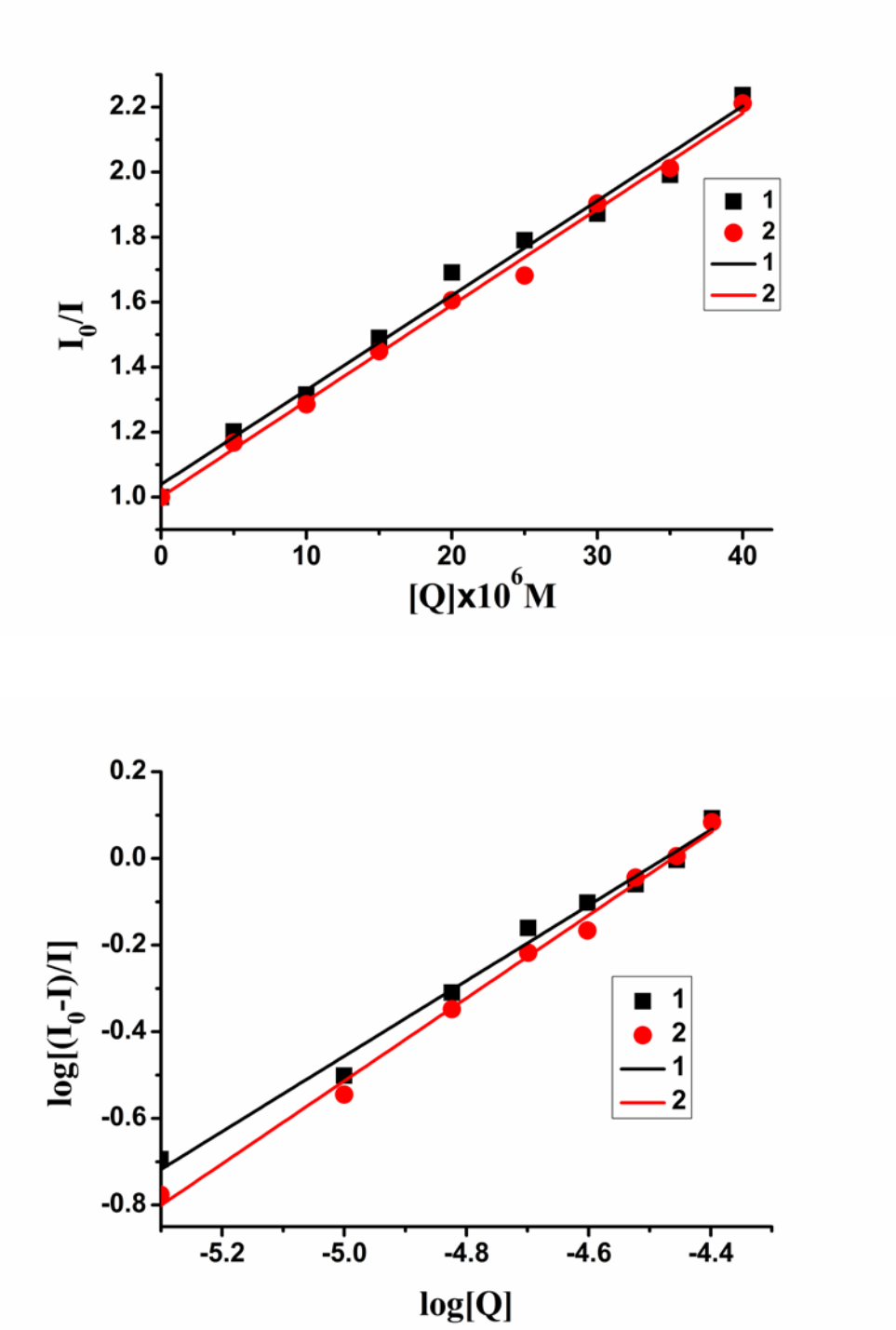

Fig. 8(a) The plot of I_0 / I versus the concentration of complex **1-2**. **(b)** Plot of $\log(I_0 - I) / I$ vs. log [Q] for BSA in the presence of complex **1-2**. (**1**(■), **2**(●))

Table 5 The quenching constants, binding constants and number of binding sites for the interaction of complex **1**-**2** with BSA.

Complex	$K_{sv}(M^{-1})$	$K_q\ (M^{-1}.s^{-1})$	$K\ (M^{-1})$	n
1	2.91×10^{4}	2.91×10^{12}	7.9×10^{3}	0.87
2	2.97×10^{4}	2.97×10^{12}	1.82×10^{4}	0.96